

# Analysis of Unsteady Aerodynamics of a Car Model with Radiator in Dynamic Pitching Motion using LS-DYNA<sup>®</sup>

Yusuke Nakae<sup>1</sup>, Jiro Takamitsu<sup>1</sup>, Hiroshi Tanaka<sup>1</sup>, Tsuyoshi Yasuki<sup>1</sup>

<sup>1</sup> Toyota Motor Corporation

## 1 Introduction

Recently, it is becoming clear that unsteady aerodynamic forces produced due to vehicle dynamic motions affect vehicle dynamic performance attributes such as straight-line stability or handling characteristics [1]. To clarify the impacts of these forces on vehicle dynamic performance attributes and their mechanisms, various experimental researches are being conducted. However, it is difficult to measure these forces in wind tunnel tests where a vehicle is stationary and is subjected to a uniform flow. Consequently, the details of the phenomenon have yet to be clarified.

Numerical simulation is expected to prove effective in revealing the detailed mechanisms of unsteady flow fields around vehicle in dynamic motion and their impacts on vehicle dynamic performance attributes. Nakae et al. [2] have conducted a numerical analysis of unsteady flow fields in the dynamic pitching motion and the lane-change maneuvering of a simplified car model simulating a vehicle by applying the Arbitrary Lagrangian-Eulerian (ALE) method to a Large-Eddy Simulation (LES) on an academic CFD code. Furthermore, Nakae et al. [3] have applied LS-DYNA ICFD solver to similar analysis. Both studies concluded that the unsteady aerodynamic forces produced due to vehicle dynamic motions were mostly induced by changes of flow structures around the front wheel house and under the car floor that changed with vehicle motion.

However, such numerical studies have been conducted on the simplified scale car model that had no engine compartment and underside components that seem to affect the flow fields. It is known that the cooling-air flow passing through engine compartment, radiator, and outlets located in front wheel house and near the floor tunnel interferes with external flow. This interference affects aerodynamic characteristics of cars. Baeder et al. [4] have investigated cooling-air interference-effects on car models. They have shown that the surface pressure distribution of the model was changed due to with or without cooling-air and also cooling-air mass flow rate. This indicates that to simulate unsteady flow fields around a vehicle in dynamic motion more precisely, installing engine compartment containing a radiator and underside components onto a car model, and considering the cooling-air effects are needed.

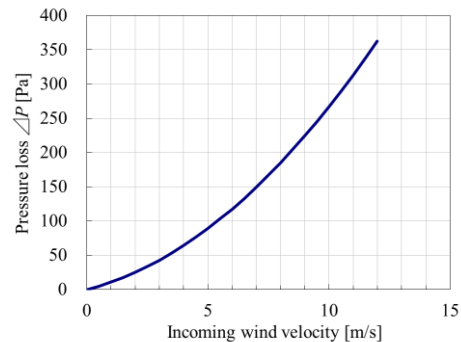
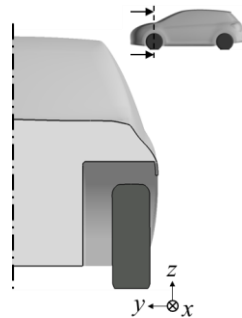
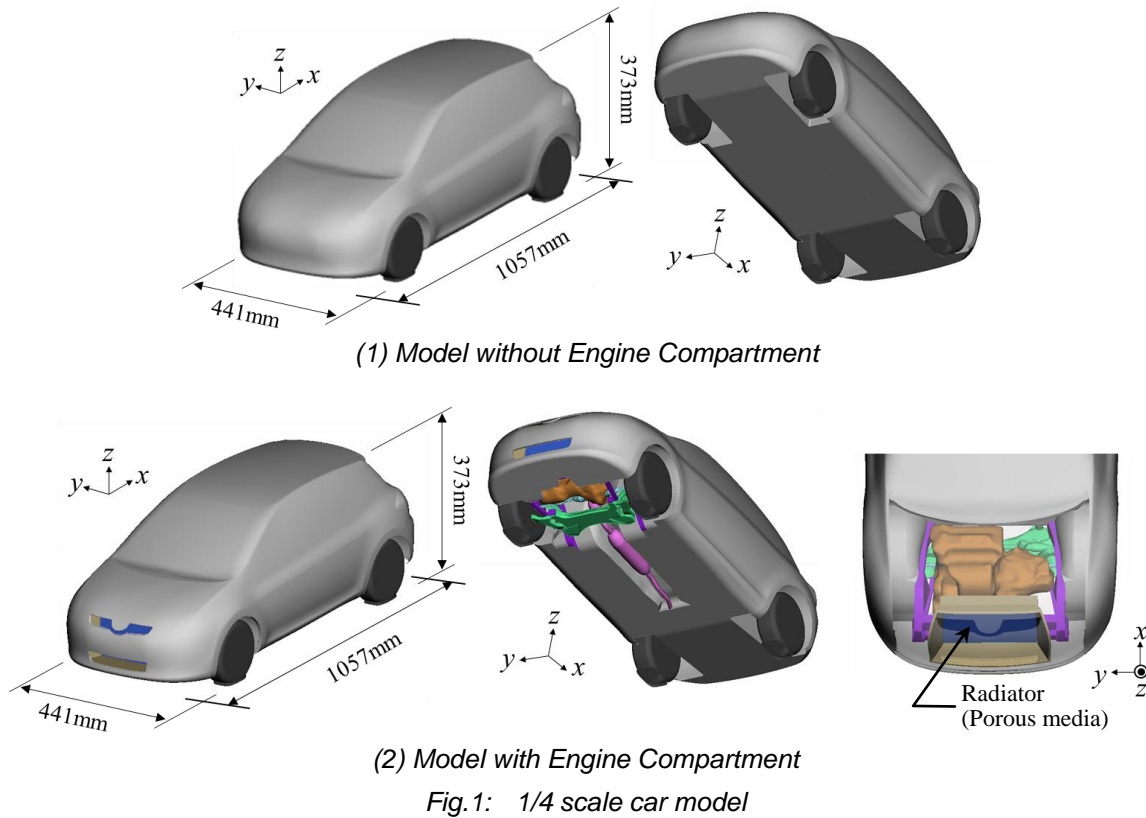
In this study, numerical simulations of the car models without or with an engine compartment containing a radiator (i.e. porous media) in stationary state and in dynamic pitching motion are performed using new porous media computing function on LS-DYNA ICFD solver. The effects of the cooling-air flow passing through engine compartment on the unsteady aerodynamic forces and the flow fields are discussed. And the necessity for installing engine compartment containing a radiator and underside components onto a car model to get closer to actual car conditions is also shown.

## 2 Object of this study

In this section, car models used in this study, simulation cases, and motion of the car model are shown.

### 2.1 Car model geometry

To investigate the cooling-air effects, two types of models shown in Fig. 1 were used. One has no engine compartment, underside components, and the suspension, same as the model in the literature [3]. The other has engine compartment containing a radiator (i.e. porous media), front suspension, and floor tunnel. Both of them are 1/4 scale car model. The models have a total length ( $L$ ) of 1057 mm, a width ( $W$ ) of 441 mm and a height ( $H$ ) of 373 mm. The model was obtained by smoothing the body surface relative to that of a real production car. The tires and body are independent, and the variations in the gap between the wheel houses and the tires when the vehicle is in dynamic motion were simulated (see Fig. 2). The porous property of the radiator for the model with engine compartment was defined using Pressure-Velocity experimental data shown in Fig. 3.



## 2.2 Simulation cases

Table 1 shows the simulation cases. The simulation cases were made for two cases of stationary state and two pitching motion cases. In all cases, mainstream velocity was 27.78 m/s, and the Reynolds number, which is based on the total length of the model, was  $Re = 1.91 \times 10^6$ . To represent the pitching motion, forced sinusoidal pitching oscillation was imposed on the model body using the center of the wheel base as the center of rotation (see Fig. 4). The effects of the cooling-air flow on the unsteady aerodynamic forces and the flow field are examined by comparing the results of the above simulations for the model with engine compartment and without it.

Table 1: List of simulation case

	Motion	Engine compartment	Pitch angle $\theta$	Velocity	Schematic view
Case 1	<b>Stationary state</b>	without	$0^\circ$	27.78 m/s	
Case 2		with			
Case 3	<b>Pitching oscillation</b>	without	$\pm 1.32^\circ$		
Case 4		with			

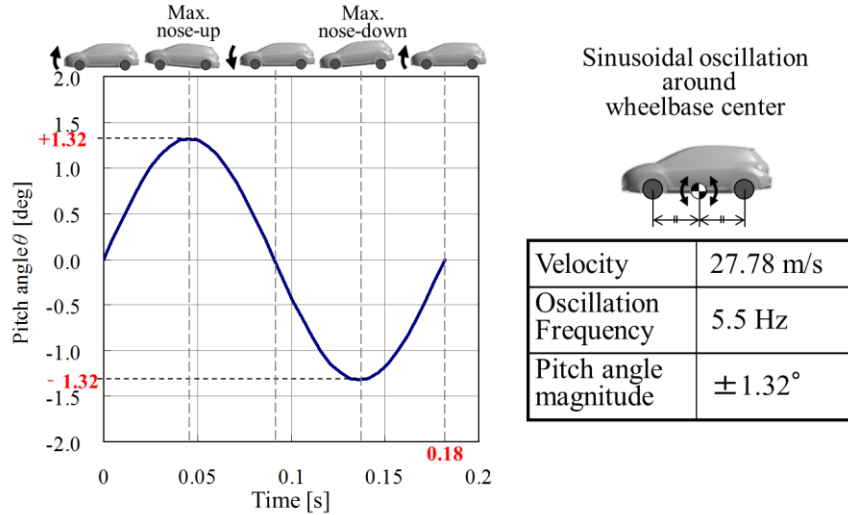


Fig.4: Behavior of model in pitching oscillation (Case 3,4)

### 3 Numerical method

The ICFD solver on LS-DYNA was used in this study. A Large-Eddy Simulation (LES) was used to model turbulent components. And the Arbitrary Lagrangian-Eulerian (ALE) method was used to represent the car model motion. Furthermore, the porous media computing function was also used to compute the flow field in the radiator.

#### 3.1 Governing equations

A spatially filtered Navier-Stokes equation (1) and a mass continuity equation (2) were used as the governing equations,

$$\rho \left( \frac{\partial \tilde{U}_i}{\partial t} + (\tilde{U}_j - v_j) \frac{\partial \tilde{U}_i}{\partial x_j} \right) = - \frac{\partial \tilde{P}}{\partial x_i} + \frac{\partial}{\partial x_j} \left[ \mu \frac{\partial \tilde{U}_i}{\partial x_j} + \mu_{sgs} \frac{\partial \tilde{U}_i}{\partial x_j} \right] \quad (1)$$

$$\frac{\partial \tilde{U}_i}{\partial x_i} = 0 \quad (2)$$

where  $t$ ,  $x_i$ ,  $U_i$ ,  $v_i$ ,  $P$ ,  $\rho$ , and  $\mu$  respectively represent, time, coordinate components, velocity components, grid movement velocity components, pressure, air density, and the viscosity coefficient. Variables marked with a  $\sim$  symbol are spatially filtered, which means that they are grid scale component variables. Further,  $\mu_{sgs}$  is the sub grid scale turbulent eddy viscosity coefficient and modeled by the Smagorinsky model shown in equation (3). The Smagorinsky constant  $C_S$  used in this study is 0.18.

$$\mu_{sgs} = \rho (C_S f_v \Delta)^2 \sqrt{2 \tilde{S}_{ij} \tilde{S}_{ij}} \quad (3)$$

$$C_S = 0.18 \quad (4)$$

In the above equations, the rate of strain tensor  $S_{ij}$  and the Van Driest wall damping function  $f_v$ ,  $\Delta$  are defined as below.

$$\tilde{S}_{ij} = \frac{1}{2} \left( \frac{\partial \tilde{U}_j}{\partial x_i} + \frac{\partial \tilde{U}_i}{\partial x_j} \right) \quad (5)$$

$$f_v = 1 - \exp \left( \frac{-y^+}{25} \right) \quad (6)$$

$$\Delta = (\text{element volume})^{\frac{1}{3}} \quad (7)$$

The  $y^+$  is the non-dimensional wall distance.

In the porous media region, cooling-air drag by radiator is added to the right side of the eq.(1) as external force  $D_i$ , which is calculated based on the Darcy-Forchheimer law.

$$\frac{\rho}{\varepsilon} \left( \frac{\partial \tilde{U}_i}{\partial t} + (\tilde{U}_j - v_j) \frac{\partial \tilde{U}_i}{\partial x_j} \right) = -\frac{1}{\varepsilon} \frac{\partial \tilde{P}}{\partial x_i} + \frac{1}{\varepsilon} \frac{\partial}{\partial x_j} \left[ \mu \frac{\partial \tilde{U}_i}{\partial x_j} + \mu_{sgs} \frac{\partial \tilde{U}_i}{\partial x_j} \right] - D_i \quad (8)$$

$$D_i = \frac{\mu \tilde{U}_i}{\kappa} + \frac{F \varphi |\tilde{\mathbf{U}}|}{\sqrt{\kappa}} \tilde{U}_i \quad (9)$$

Where  $\varepsilon$ ,  $\kappa$ , and  $F$  respectively represent, porosity, permeability, and Forchheimer inertia parameter of porous media. In this study,  $\varepsilon$  was set to 1.0,  $\kappa$  and  $F$  were calculated based on the Pressure-Velocity experimental data shown in Fig. 3. Anisotropy of flows through radiator by radiator fins was not considered.

The fractional step method was used to solve these equations.

### 3.2 Validation of porous media computation

Before conducting the simulations of the car model with radiator, a validation of porous media computing function on LS-DYNA ICFD solver was carried out with radiator unit simulation. The computational domain for this validation is shown in Fig. 5. A radiator is located at the middle section of the domain. Dimensions, characteristics of the radiator, and mesh size around the radiator are the same as those in the simulations of the car model with radiator (Case 2,4). The incoming wind velocity imposed at inlet is shown in Fig.6. To validate pressure differences ( $\Delta P$ ) between in front of a radiator and behind of it at various wind velocity, the incoming wind velocity was changed as time progresses.

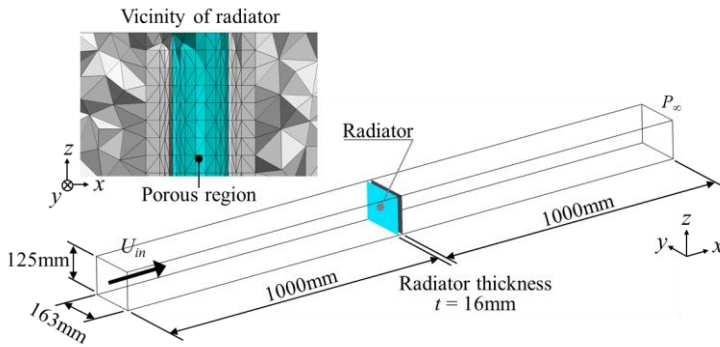


Fig.5: Computational domain for validation of porous media computation

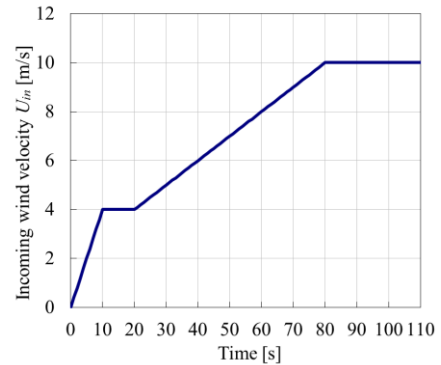


Fig.6: Incoming wind velocity

Fig.7 shows the computational result of the pressure difference ( $\Delta P$ ) between in front of the radiator and behind of it. The result showed the error within 5% from the theoretical value. This indicates the validity of this porous media computing method.

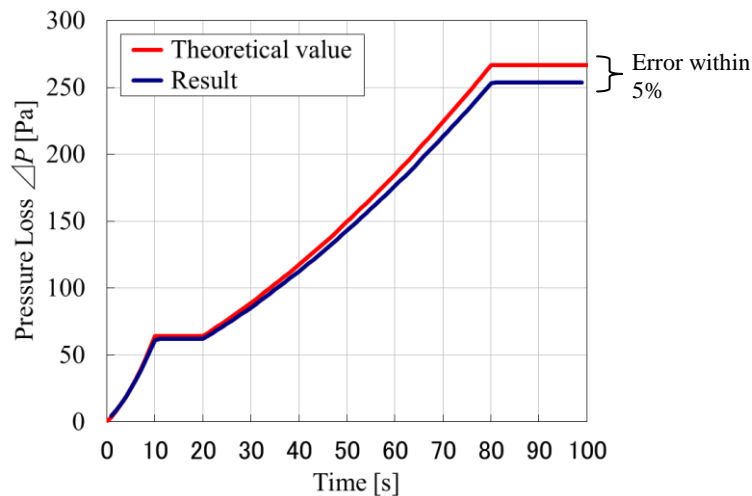


Fig.7: Comparison between result of computation and theoretical value

#### 4 Numerical conditions

Fig. 8 shows the computational domain for Case 1 through 4. Dimensions are indicated in reference to  $L$ , the total length of the model. Flow direction is  $10L$ , width direction is  $2L$  and height direction is  $1.5L$ . Fig. 9 shows the model surface and the computational grid in its vicinity. The computational grid for the model surface has a resolution of approximately 4 mm, and a 5-layer boundary layer mesh was inserted in the model surface as well as in the floor of the computational domain. The first layer has an approximate height of  $y^+ = 3.5$ . The entire computational domain consists of unstructured tetrahedral grids using a total of 13.6 million elements and 2.3 million nodes.

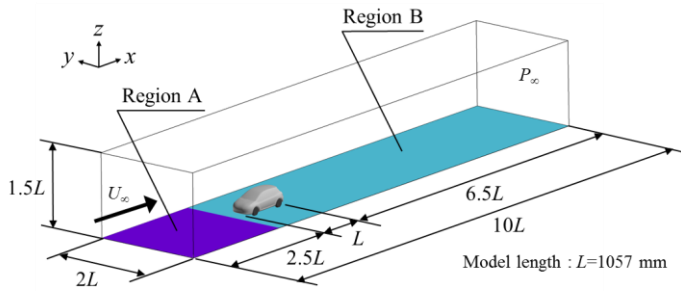


Fig.8: Computational domain

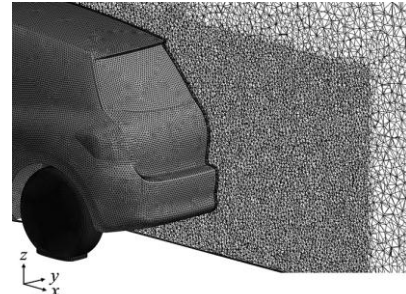


Fig.9: Close-up view of computational grid

Boundary conditions are presented in Table 2. They are the same across all simulation cases.

Table 2: List of boundary condition

Boundary	Condition
Inlet	Uniform velocity $U_\infty = 27.78$ [m/s]
Outlet	Constant pressure $P_\infty = 0$ [Pa]
Floor	Region A : Free-slip, Region B : Non-slip
Side walls, Ceiling	Free-slip
Model surface	Non-slip, 5 layers of boundary layer meshes

#### 5 Results

In this section, the computational results for Case 1 through 4 are shown. Firstly, differences between flow fields around the car model with engine compartment containing the radiator and that without engine compartment in stationary state are shown to reveal the effects of the cooling-air flow passing through engine compartment. Secondly, difference in unsteady aerodynamic force during pitching motion between these two models is showed.

##### 5.1 Stationary case (Case 1 and 2)

Fig. 10 through 14 respectively show the differences between the car model without engine compartment (Case 1) and that with engine compartment (Case 2) in the surface pressure distribution on the upper and lower side of the model body at the center cross-section, the volume flow rate under the model body, the spatial averaged total pressure of each  $y$ - $z$  plane under the model body, and the total pressure distribution under the model body at a  $x$ - $y$  plane. And also the results of the full scale real production car which is original shape of the models in this study with opened radiator grille and closed grille by another CFD code are shown simultaneously to validate the results of this computations. The model of real production car and CFD solver are the same as those in literature [5].

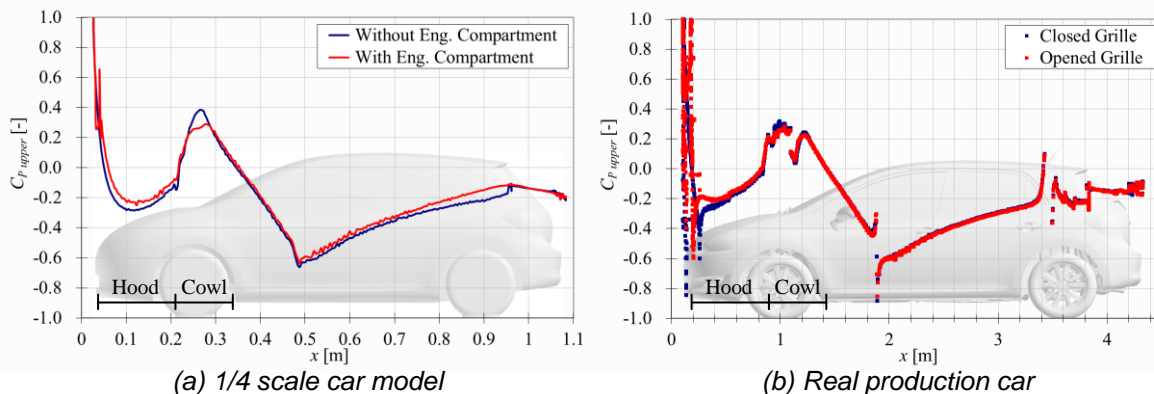
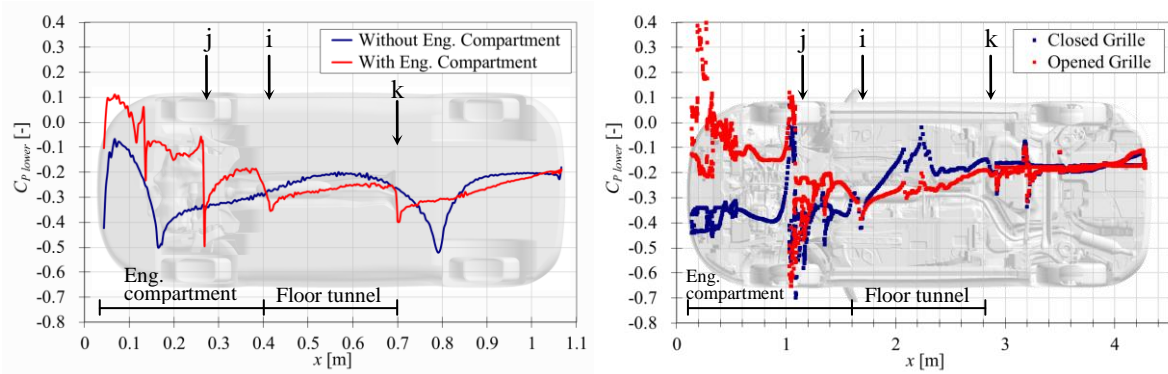
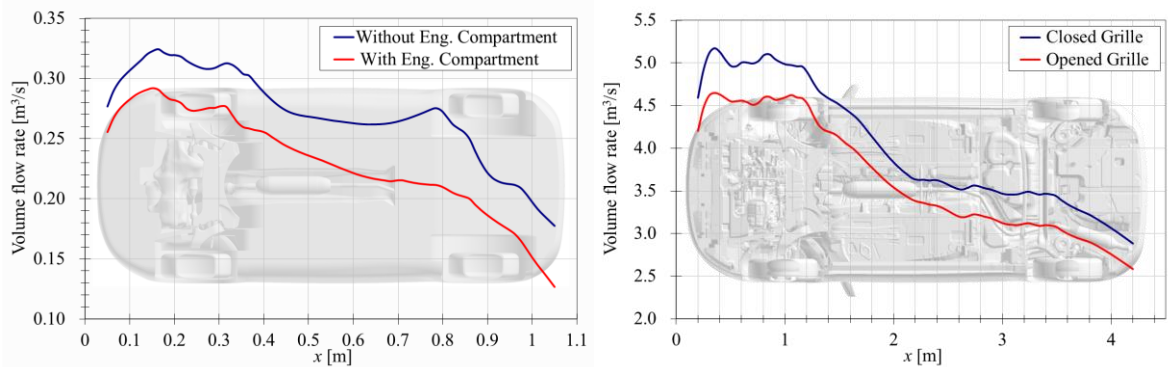


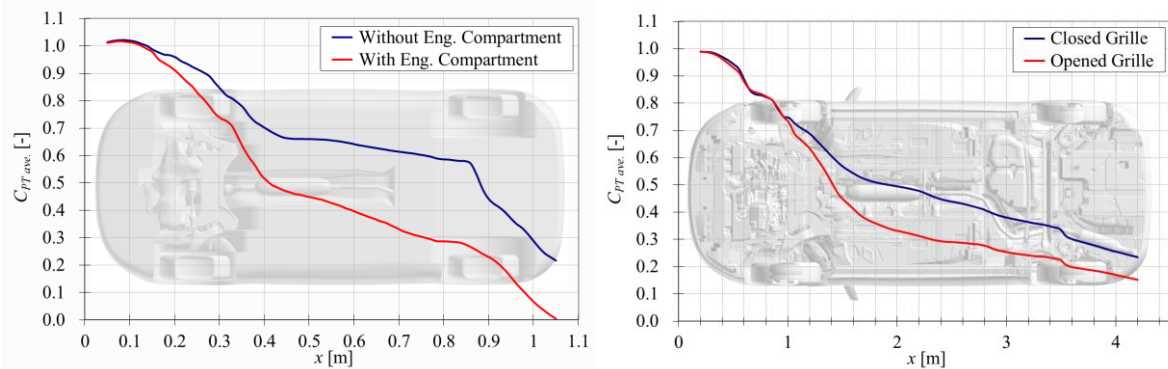
Fig.10: Surface pressure distribution on upper body at center cross-section



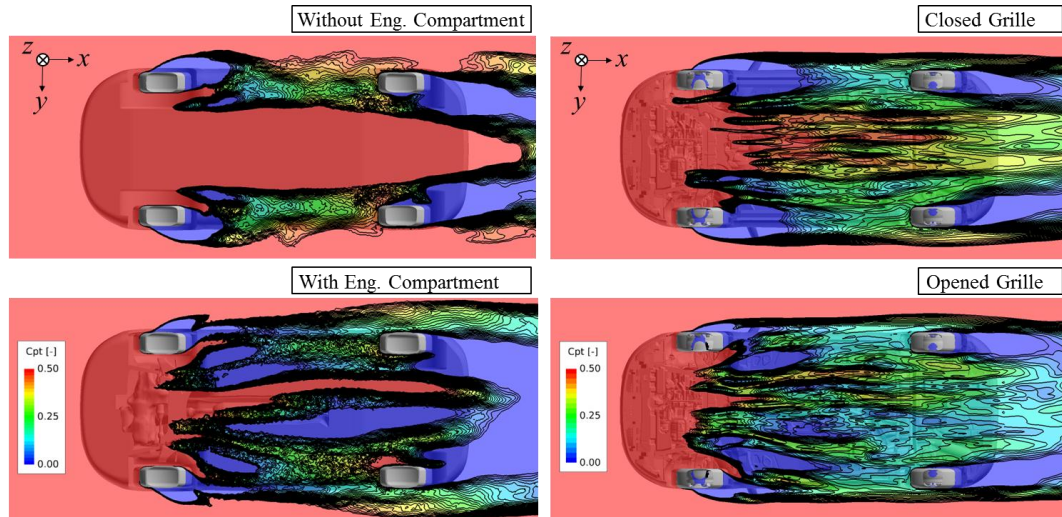
(a) 1/4 scale car model (b) Real production car  
 Fig.11: Surface pressure distribution on lower body at center cross-section



(a) 1/4 scale car model (b) Real production car  
 Fig.12: Volume flow rate under body



(a) 1/4 scale car model (b) Real production car  
 Fig.13: Spatial averaged total pressure under body



(a) 1/4 scale car model (b) Real production car  
 Fig.14: Total pressure distribution under body

The results indicate the time averaged values for 0.7 second after sufficient convergence of the computations.

For the surface pressure distribution on the upper side (Fig.10), in the case of the model with engine compartment, the higher pressure on the engine hood and lower pressure on the windshield cowl than that on the model without engine compartment were observed. Remarkable differences in the surface pressure distribution were observed on the lower side of the model body (Fig. 11). In the case of the model with engine compartment, significant higher pressure on the front part (forward than  $x = 0.4$ ) where the engine compartment is located was observed. Furthermore, lower pressure behind there (behind  $x = 0.4$ ) where the floor tunnel is located was also observed. This sudden pressure change was occurred where the cooling-air outlet (i.e. the outlet located between rear end of the engine compartment and front end of the floor tunnel : i in Fig. 11) is located. Other negative pressure peaks located at  $x = 0.3$  and  $0.7$  also correspond to the location of the outlet between bottom of the engine block and the front suspension member (j in Fig. 11), and rear end of the floor tunnel (k in Fig.11) respectively.

The volume flow rate under the model body with engine compartment decreased compared to the case of the model without engine compartment (Fig. 12).

The total pressure under the model body with engine compartment gradually decreased around  $x = 0.27$  and drastically decreased around  $x = 0.4$  compared to the model without engine compartment (Fig. 13). The locations where these changes occurred correspond to the location where the cooling-air outlets mentioned in Fig. 11 are located.

The total pressure distribution under the model body with engine compartment decreased from under the engine compartment. Especially, decreases from where the outlets are located were remarkable. These decreases correspond to Fig. 13.

All of the differences between the model with engine compartment and that without engine compartment described above was also observed in the results of the real production car with opened radiator grille and closed grille (Fig. 10(b) through 14(b)).

## 5.2 Dynamic case (Case 3 and 4)

Fig. 15 shows the computational results for unsteady aerodynamic force during the pitching motion. The results indicate the phase averaged value for five cycles after sufficient convergence of the computations. The most remarkable unsteadiness in aerodynamic forces relative to vehicle dynamic motion was observed in the lift force. This report focuses on the lift coefficient  $C_L$  which seems to affect the vehicle dynamic performance attributes. The  $C_L$  during nose-down motion showed significant difference while it showed a consistent close correspondence during nose-up motion between the model with engine compartment and that without engine compartment. The  $C_L$  acting on the model with engine compartment showed higher value than that without engine compartment only during nose-down motion. This indicates that evaluations using the car model without engine compartment have possibilities of overestimating the amplitude of unsteady aerodynamic forces than the forces acting on a real production car in dynamic motion.

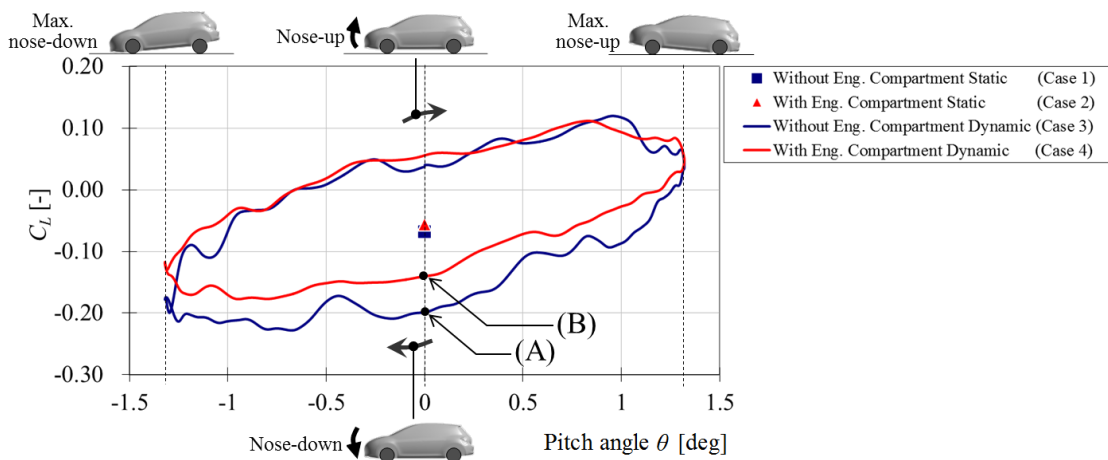


Fig. 15: Unsteady aerodynamic force during pitching motion

To pinpoint the cause of the above-mentioned difference in aerodynamic force, the  $C_L$  acting on each part of the model body for nose-down at pitch angle  $0^\circ$  where the most remarkable difference occurred between the models ((A), (B) in Fig. 15) are presented in Fig. 16. These results revealed that the body

part which have contributed to the increase in  $C_L$  for the model with engine compartment was most remarkably under the engine compartment and the front wheel house (FLR-1,FWH).

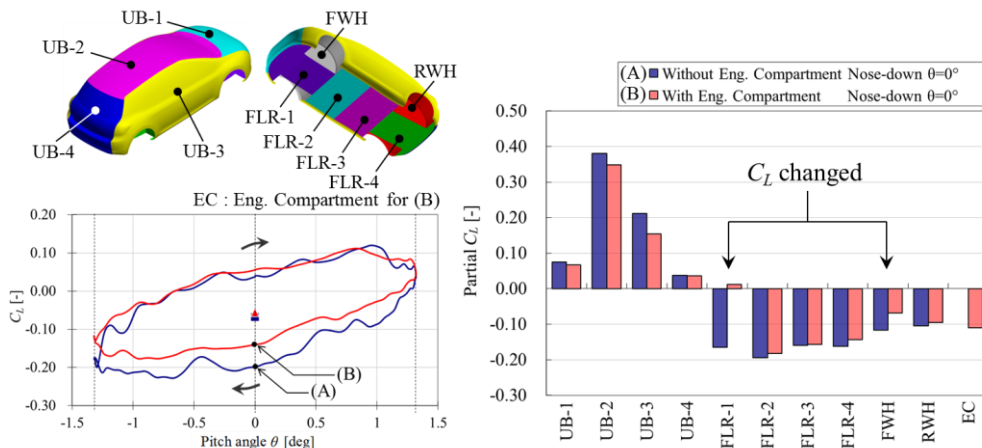


Fig.16: Aerodynamic force  $C_L$  acting on each part of model body

## 6 Discussion

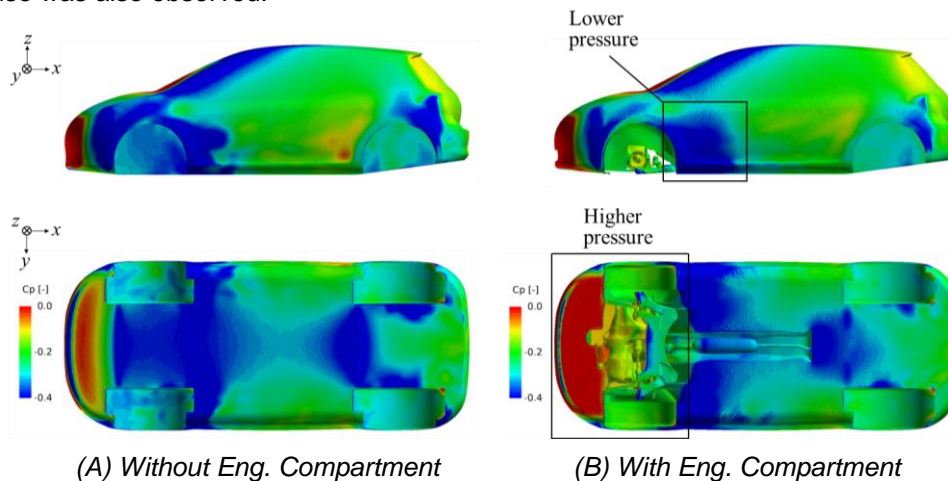
In this section, the effects of the cooling-air flow passing through engine compartment on the flow fields and the unsteady aerodynamic force are discussed. Through this discussion, the necessity for installing engine compartment containing a radiator and underside components onto a car model to get closer to actual car conditions is also shown.

### 6.1 Stationary case (Case 1 and 2)

As shown in section 5.1, the surface pressure on the lower side of the model body with engine compartment obviously changed where the cooling-air outlets are located. The upstream of the outlets, the surface pressure is higher than that in downstream. Furthermore, the volume flow rate and the total pressure under the model body decreased from the location. These indicate that the cooling-air flow passing through engine compartment obviously disturbs (interferes with) the flow under the model body. And this leads to the change of flow under the body and finally affects the aerodynamic characteristics of a car. These were also observed in the real production car. This indicates that to understand the flow fields around a vehicle more precisely, engine compartment and underside components of a car should be considered.

### 6.2 Dynamic case (Case 3 and 4)

Considering the cooling-air effect revealed in previous sections, the causes underlying the difference in the  $C_L$  during nose-down motion ((A), (B) in Fig. 15) are examined. Fig. 17 shows the surface pressure distribution on the model body for nose-down at pitch angle  $0^\circ$  ((A), (B) in Fig. 15). Same as shown in Fig. 16, remarkably higher pressure was observed under the engine compartment and on the front wheel house of the model with engine compartment than that of the model without engine compartment. Consequently, the total lift force  $C_L$  acting on the model with the engine compartment indicates higher value. In addition, difference on the front fender panel especially behind the front wheel house was also observed.



(A) Without Eng. Compartment (B) With Eng. Compartment  
Fig.17: Surface pressure distribution at pitch angle  $0^\circ$  during nose-down

Next comes an examination of the causes of the differences in the pressure distribution under the engine compartment and on the front wheel house. Fig. 18 shows the velocity magnitude distribution at the center cross-section and the x-y plane located 24mm above ground level. And Fig. 19 shows velocity magnitude at  $y = 0.035$  and 24mm above ground level. In case of the model with engine compartment, the flow velocity under the model body was remarkably lower. This originates from under the engine compartment especially the locations where the cooling-air outlets are located (i.e. between rear end of the engine compartment and front end of the floor tunnel : i in Fig. 18 and 19, between bottom of the engine block and the front suspension member : j in Fig. 18 and 19). This indicates that the cooling-air blowing from engine compartment disturbs the flow under the model body and thus the flow is decelerated and pressure increases under the engine compartment. Moreover, in the engine compartment, pressure is originally higher than that in external flow due to lower velocity of the flow in engine compartment. These two factors lead to increasing the surface pressure under the engine compartment and on the front wheel house as observed in Fig. 17. Consequently, the total lift force  $C_L$  acting on the model with the engine compartment indicates higher value.

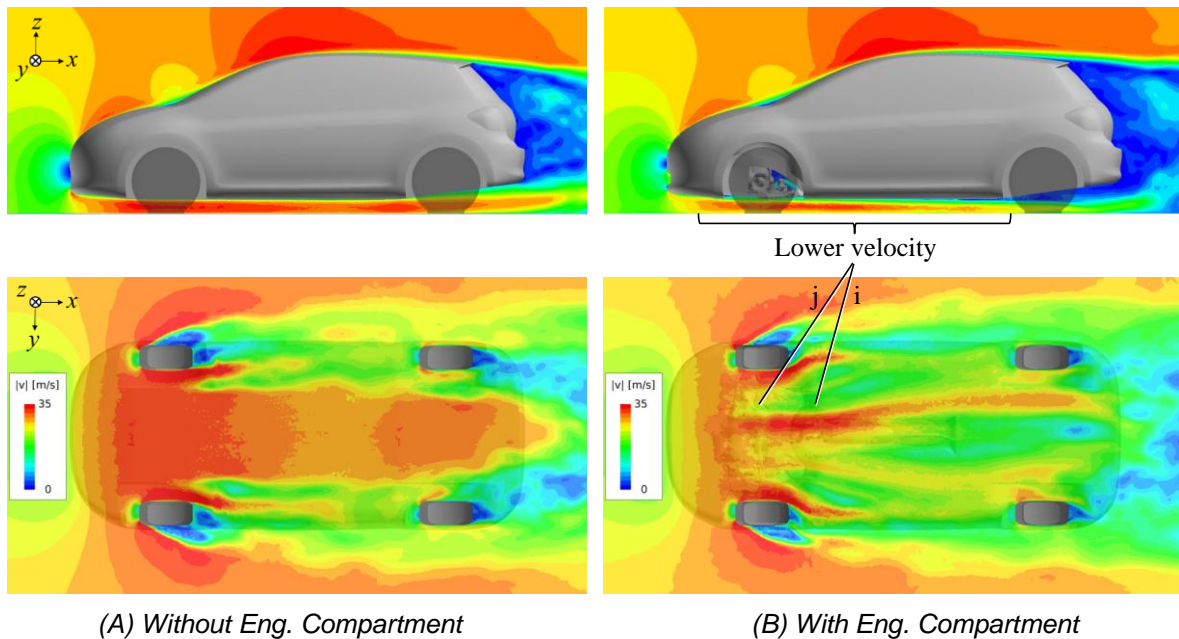


Fig. 18: Velocity magnitude distribution at pitch angle  $0^\circ$  during node-down

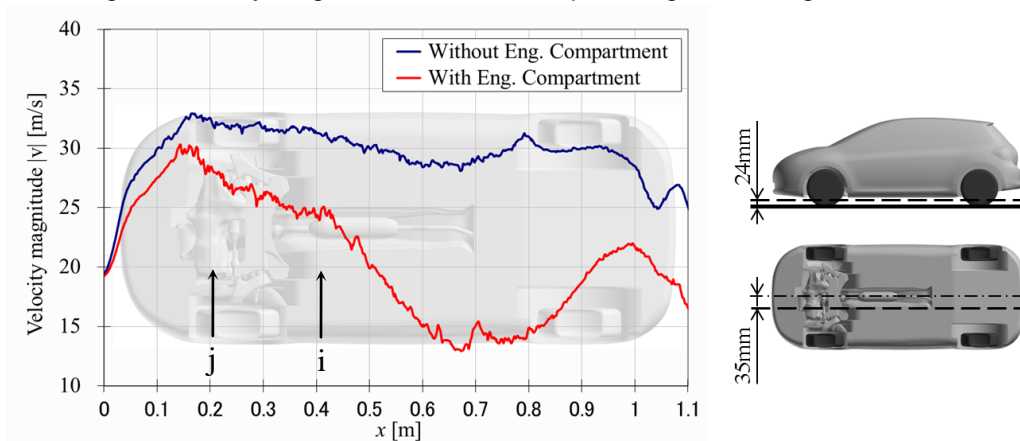
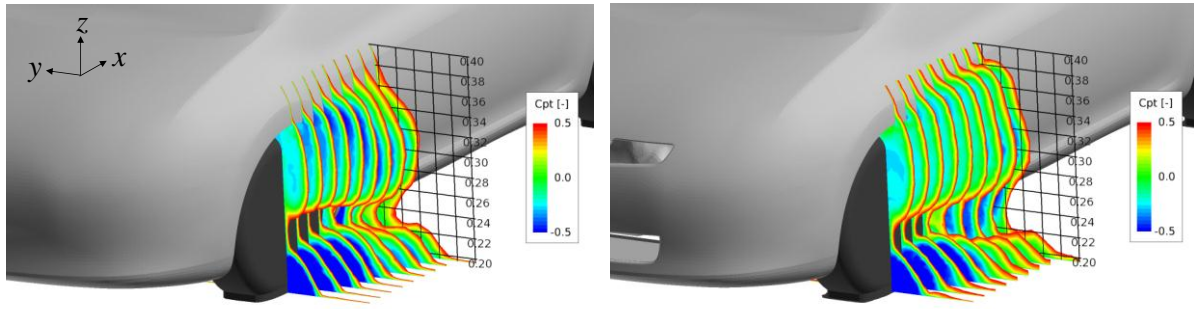


Fig. 19: Velocity magnitude at  $y = 0.035$  and 24 mm above ground level at pitch angle  $0^\circ$  during node-down

Fig. 20 shows the total pressure distribution around front wheel house. The cooling-air blowing from engine compartment also flows into front wheel house and it affects the flow field around front wheel house. In case of the model with engine compartment, the flow blowing from the front wheel house to the outside of the model body increases. Thus the wake region of front wheel house widens and it leads to decreasing the surface pressure on the front fender panel behind the front wheel house as observed in Fig.17.



(A) Without Eng. Compartment

(B) With Eng. Compartment

Fig.20: Total pressure distribution around front wheel house at pitch angle  $0^\circ$  during node-down

Fig. 21 shows the stream lines of the cooling-air flow passing through engine compartment and the radiator for the model with engine compartment. The flow out from the engine compartment strongly interferes with the external flow, especially with the flow under the body. Consequently, the differences in the flow field under the body occur and it greatly affects the aerodynamic characteristics of cars.

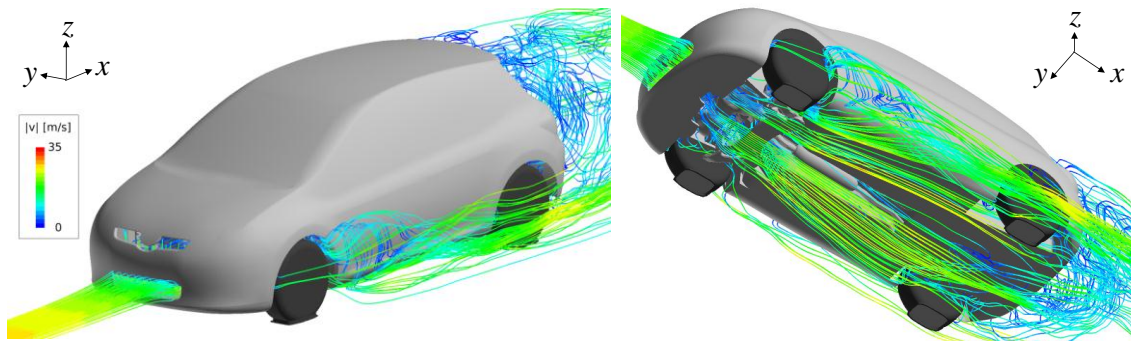


Fig.21: Cooling-airflow passing through engine compartment and radiator at pitch angle  $0^\circ$  during node-down

These mechanisms examined above are remarkably observed during nose-down motion since the flow under the model and the cooling-air are accelerated due to the body motion. While during the nose-up motion, the effect of the cooling-air is comparatively small since the flow under the model and the cooling-air are decelerated due to the body motion.

## 7 Summary

The numerical simulations of the car model with an engine compartment containing a radiator (i.e. porous media) in stationary state and in dynamic pitching motion were conducted using new porous media computing function on LS-DYNA ICFD solver. As a result of this study, the followings were made clear.

- i. The result of the porous media computation showed good agreement with the theoretical value. The validity of the porous media computing method was shown.
- ii. The effects of the cooling-air flow passing through engine compartment and radiator on the flow fields and the unsteady aerodynamic force were clarified.
- iii. The necessity for installing engine compartment containing a radiator and underside components onto a car model to get closer to actual car conditions was shown.

## 8 Acknowledgments

Thanks and appreciation are extended to extensive assistance and support with LS-DYNA provided by Mr. Amano and Mr. Hayashi of the JSOL Corporation over the course of this study.

## 9 References

- [1] Okada, Y., et al., : "Flow Structures above the Trunk Deck of Sedan-Type Vehicles and Their Influence on High-Speed Vehicle Stability 1st Report: On-Road and Wind-Tunnel Studies on Unsteady Flow Characteristics that Stabilize Vehicle Behavior", SAE Technical Paper, 2009, 2009-01-0004
- [2] Nakae, Y., et al., : "A Study of Unsteady Aerodynamic Forces Acting on Car in Dynamic Motion" Transactions of Society of Automotive Engineers of Japan, 2013, Vol.44, No.6, 20134862
- [3] Nakae, Y., et al., : " Analysis of Unsteady Aerodynamics of a Car Model in Dynamic pitching Motion Using LS-DYNA R7", 13th International LS-DYNA Users Conference, 2014
- [4] Baeder, D., et al., : "Aerodynamic Investigation of Vehicle Cooling-Drag", SAE Technical Paper, 2012, 2012-01-0170
- [5] Tadatsu, M., et al., : "A Study on Aerodynamic Drag Reduction of Two-Box Vehicle" Transactions of Society of Automotive Engineers of Japan, 2013, Vol.44, No.5, 20134710